LANGMUIR

pubs.acs.org/Langmuir Article

Spreading of Water Droplets on Cellulose-Based Papers: the Effect of Back-Surface Coating

Ching-Bin Lin, Han-Sen Chang, Yulin Zhang, Fuqian Yang, and Sanboh Lee*

Cite This: *Langmuir* 2021, 37, 376–384 Read Online

ACCESS | Metrics & More | Article Recommendations | Supporting Information

ABSTRACT: Regulation of wetting and spreading of liquid on porous material plays an important role in a variety of applications, such as waterproofing, anti-icing, antioxidation, self-cleaning, etc. In this work, we reveal the role of back-surface coating with superhydrophobic nanoparticles in controlling the spreading of water droplets on cellulose-based papers. A layer of superhydrophobic polydivinylbenzene (PDVB) nanoparticles is spin-coated on the back surface of different types of papers. The spreading of a water droplet on the top, uncoated surface is dependent on the size of the PDVB nanoparticles in the coating. Using a relationship derived from Darcy's law, we observe that the energy barrier for the spreading of water droplets on three types of papers (heavy-weight, light-weight, and slight-weight papers) decreases with the decrease of the nanoparticle size in the back-surface coating. The spreading of the water droplet is dependent on the porous structure, permeability, and compressibility of the papers. The method presented in this work provides a feasible approach to use the back-surface coating to control the wettability of papers.

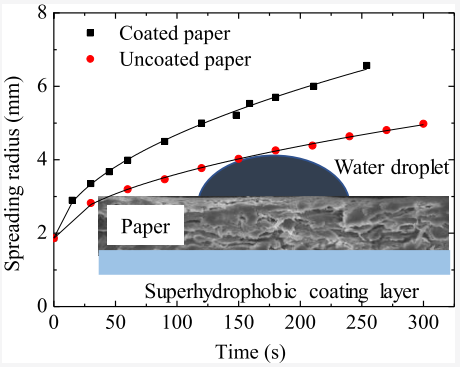

1. INTRODUCTION

Controlling the wetting and spreading of water on solid surfaces is of practical importance for a variety of applications, such as waterproofing,[1−3] anti-icing,[4,5] antioxidation,[6,7] self-cleaning,[8,9] etc. There are various techniques available to form superhydrophobic surfaces with contact angles larger than 150° and rolling angles less than 10°,[10] i.e., surfaces of low wettability. In general, these techniques can be divided into two categories: one involves surface treatment/coating, such as the use of low surface energy materials (poly(tetrafluoroethylene), silicone, etc.),[10] and the other introduces nanotextured/templated/rough surfaces. In the heart of the nanotextured/templated/rough surfaces is the regulation of the interaction between water droplets and solid surfaces.

Cellulose-based papers have been widely used in our daily life. There is a great need to control their surface characteristics for a variety of applications. Samyn[11] reviewed the techniques used in fabricating papers with hydrophobicity. Balu et al.[12] discussed the use of plasma etching and coating to obtain papers of a superhydrophobic surface. Using plasma etching and fluoropolymer coating, Li et al.[13] prepared superamphiphobic paper surfaces. By spray-coating α-cellulose 10-undecylenoyl ester on filter papers, Zhang et al.[14] obtained superhydrophobic-reactive papers. Jiang et al.[15] used debonder agents, oxygen plasma, and solution coating to control the surface structures of papers and improve the amphiphobic characteristics of papers. Most of these studies have focused on the superhydrophobic characteristics of papers.

Surface characteristics play an important role in the wetting and spreading of water droplets on papers. Han and Krochta[16] studied the wetting behavior of whey protein-coated paper and noted the change of the contact angle with the surface energy of liquid and temporal variation of the contact angle. Modaressi and Garnier[17] demonstrated the effect of chemical and physical heterogeneities on the contact angle of water droplets on sized papers. Kwon et al.[18] examined the wetting of a plain white paper towel and revealed the self-affine fractal feature of the wetting. Gillespie[19] examined the spreading of the stains carried by low vapor pressure liquids in the filter paper and the printflex card, while he did not analyze the temporal evolution of the droplet size. Rosenholm[20] investigated the liquid spreading on coated and uncoated papers and suggested the power law relationship between the spreading size and the spreading time. However, there are few studies focusing on the effects of back-surface coating and temperature on the spreading and wetting of water droplets on papers.

Considering the applications of cellulose-based papers in a variety of areas, we study the effects of back-surface coating and temperature on the spreading of water on the uncoated surface of the papers with and without back-surface coating. Superhydrophobic polydivinylbenzene (PDVB) nanoparticles

Received: October 14, 2020
Revised: November 22, 2020
Published: December 30, 2020

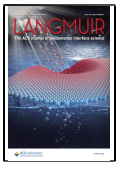

https://dx.doi.org/10.1021/acs.langmuir.0c02991
Langmuir 2021, 37, 376−384

are used in the back-surface coating of the papers. The focus is on the temporal evolution of the droplet sizes and the temperature dependence of the spreading behavior.

2. EXPERIMENTAL DETAILS

Both coated and uncoated papers were used in this work. The coated papers were obtained from Dayeh Holding Enterprise Co. (New Taipei City, Taiwan), and the uncoated papers were obtained from Hsinchu Paper Factory (Hsinchu, Taiwan). Tables S1 and S2 list the information of the papers and the abbreviations used in this work. The grammage was 84.8 g/m^2 for all of the papers except the wood-free papers, whose grammages were 53, 80.4, and 159 g/m^2.

Following the approach given by Chang,[21] we used the solvothermal process to prepare superhydrophobic PDVB nanoparticles. Briefly, a solution consisting of 18 g of divinylbenzene and 0.45 g of azobisisobutyronitrile (AIBN) in 180 g of ethyl acetate was first prepared. The solution was placed in an autoclave liner to a 70% capacity, which was heated to 100 °C and maintained at 100 °C for 36 h under a pressure of 208 atm. The product collected from the autoclave liner was stored in a vacuum oven at 50 °C under 10^{-3} Torr for 8 h to remove the residual of ethyl acetate. The chemical compound obtained was then ground to powder. An alcohol suspension with 2 wt % of the prepared powder was sonicated for 8 h to produce PDVB nanoparticles, which was named as PDVB-NPs. PDVB-NPs of different molecular weights were produced using different amounts of AIBN (0.045, 0.45, and 4.5 g). The corresponding compounds were denoted as PDVB-*x*, where *x* is the amount of AIBN used in the solvothermal process.

Spin-coating was used to coat a layer of PDVB-NPs on surfaces of the papers of 5 × 5 cm^2 in area. The suspension for the spin-coating was 50 μL of an alcohol solution made from the prepared PDVB-NPs. The spin speeds were 400, 600, and 800 rpm, which controlled the coating thickness.

The morphology of the PDVB-NPs and the microstructures of the papers with a layer of PDVB-NPs were analyzed using a scanning electron microscope (SEM; JSM-7610F, JEOL, Tokyo, Japan). Gold coating was performed over PDVB-NPs and the coating layer at 10 mA for 120 s prior to the SEM imaging. The composition of the coating layers was determined using an energy-dispersive X-ray spectroscope (Oxford-model 6209, Oxford Instruments, Oxford, U.K.) attached on a JSM-7610F (JEOL, Tokyo, Japan).

The size distribution of the PDVB-NPs was measured using a dynamic light scattering instrument (Malvern, Worcestershire, U.K.) at 25 °C. The suspensions, which consisted of 10 mg of PDVB-NPs in 10 mL of ethanol, were sonicated for 5 min prior to the size measurement. Three measurements were performed for individual PDVB-NPs.

Contact angles of liquid droplets on the coating layer were measured using an FTA 125 contact angle instrument (First Ten Angstroms Inc., Portsmouth, VA) at 25 °C. The volume of the water droplets was 4 μL and the relative humidity was 52%.

The molecular weight of the PDVB-NPs was determined from the viscosity measurement. This is because it is difficult to use gel permeation chromatography to measure the molecular weight of PDVB, which is associated with the insolubility of PDVB. The dynamic viscosity of PDVB-NP solutions was measured using a Cannon-Ubbelohde 6963S glass viscometer (Ramin, Houston, TX) at 25 °C. The PDVB-NP solutions consisted of PDVB-NPs of different weight percentages (0.005, 0.01, 0.015, and 0.02 wt %) in divinylbenzene.

The chemical structures of the PDVB-NPs were analyzed on a Fourier transform infrared (FT-IR) spectrometer (Vertex 80 v, Bruker Corporation, Billerica, MA). The spectra wavenumber for the measurements was in a range of 4000−600 cm^{-1}.

Spreading of water droplets on the uncoated surface of the papers, whose backside was coated with a PVDB-NP layer, as shown schematically in Figure 1, was performed at 25 °C. DI water (5 μL) was dripped on the uncoated surface. The sizes of the water droplets were recorded by a digital camera. The temporal evolution of the spreading sizes was analyzed by ImageJ (National Institute of Health, Bethesda, MD). The papers used in the spreading tests were HW-coated paper, LW-coated paper, SW-coated paper, wood-free paper, text paper, printing paper, and white newspaper. The grammages for the 50P, 80P, and 150P wood-free papers were 53, 84.8, and 159 g/cm^2, respectively. Here, HW, LW, and SW represent heavy weight, light weight, and slight weight, respectively.

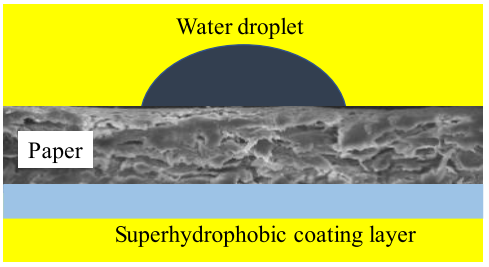

Figure 1. Schematic of the spreading of a water droplet on the uncoated surface of a paper with a coated backside.

3. RESULTS AND DISCUSSION

Figure 2 shows SEM images of PDVB-0.045, PDVB-0.45, and PDVB-4.5 and the PDVB coating layers. It is evident that the combination of the solvothermal processing and mechanical grinding indeed produced nanosized particles (Figure 2a−c) for the amounts of AIBN used in this work. The spin-coating of the nanoparticle-based solutions formed a layer of nanoparticles on the surface of the papers, as shown in Figure 2d.

Figure 3 depicts the size distribution of PDVB-NPs, as measured by the dynamic light scattering technique. There are two peaks; the one with a smaller size is less than 12 nm, and the one with a larger size is larger than 50 nm. According to the SEM images in Figure 3, we expect that the particle sizes are less than 50 nm. That is to say, the peak centered at a larger size represents the aggregates of PDVB-NPs, and the peak centered at a smaller size likely represents the size distribution of the PDVB-NPs. Using the peak centered at a smaller size, we obtain the average particle sizes of 14.74 ± 1.12, 5.31 ± 0.37, and 1.10 ± 0.08 nm for PDVB-0.045, PDVB-0.45, and PDVB-4.5, respectively. Increasing the fraction of AIBN decreases the average size of the nanoparticles. Note that the peaks for the aggregates of the PDVB-NPs are at ∼480, ∼60, and ∼2500 nm for PDVB-0.045, PDVB-0.45, and PDVB-4.5, respectively.

Figure 4 presents the FT-IR spectrum of the PDVB-NPs under an attenuated-total reflection (ATR) mode. The peaks centered at wavenumbers of 708, 794, 829, 900, 1446, 1486, 1604, and 2926 cm^{-1} have been reported by Jafari et al.[22] and Nuasaen and Tangboriboonrat.[23] The peaks with wavenumbers in the range of 700−950 cm^{-1} represent the C−H bending of alkene groups, and the peaks with wavenumbers in the range of 1430−1510 cm^{-1} are related to the C═C stretching mode of benzene groups. The peak centered at 1604 cm^{-1} represents the C═C stretching mode of alkene groups. The peaks with wavenumbers in the range of 2850−3100 cm^{-1} consist of the CH stretching vibration of both alkene groups and benzene groups. All of the peaks correspond to the bands of divinylbenzene. Thus, we can conclude that the monomer for the formation of PDVB-NPs is divinylbenzene and the combination of the solvothermal processing and mechanical grinding indeed produced PDVB-NPs.

https://dx.doi.org/10.1021/acs.langmuir.0c02991
Langmuir 2021, 37, 376−384

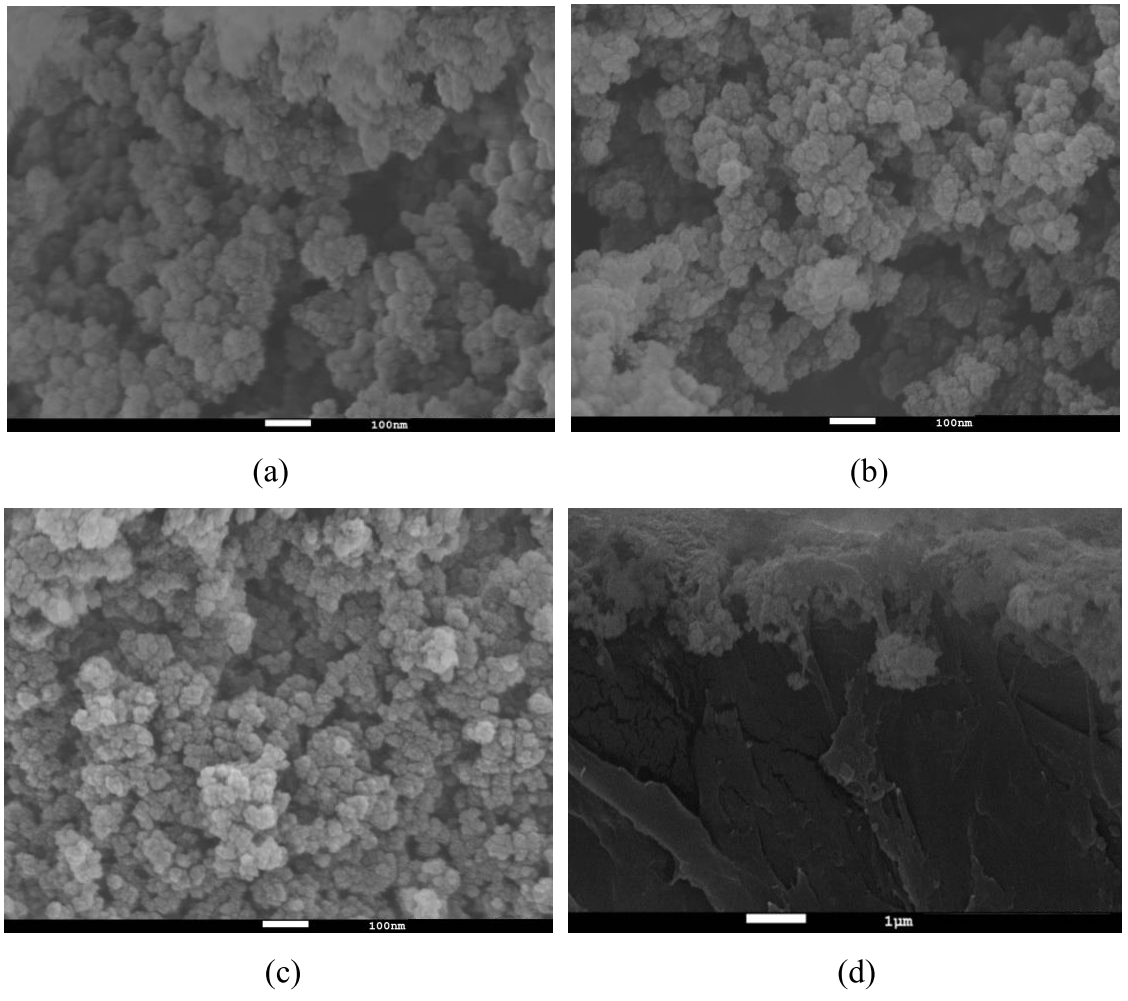

Figure 2. SEM images of PDVB-NPs and the PDVB-NP film; (a) PDVB-0.045, (b) PDVB-0.45, (c) PDVB-4.5, and (d) PDVB-NP films.

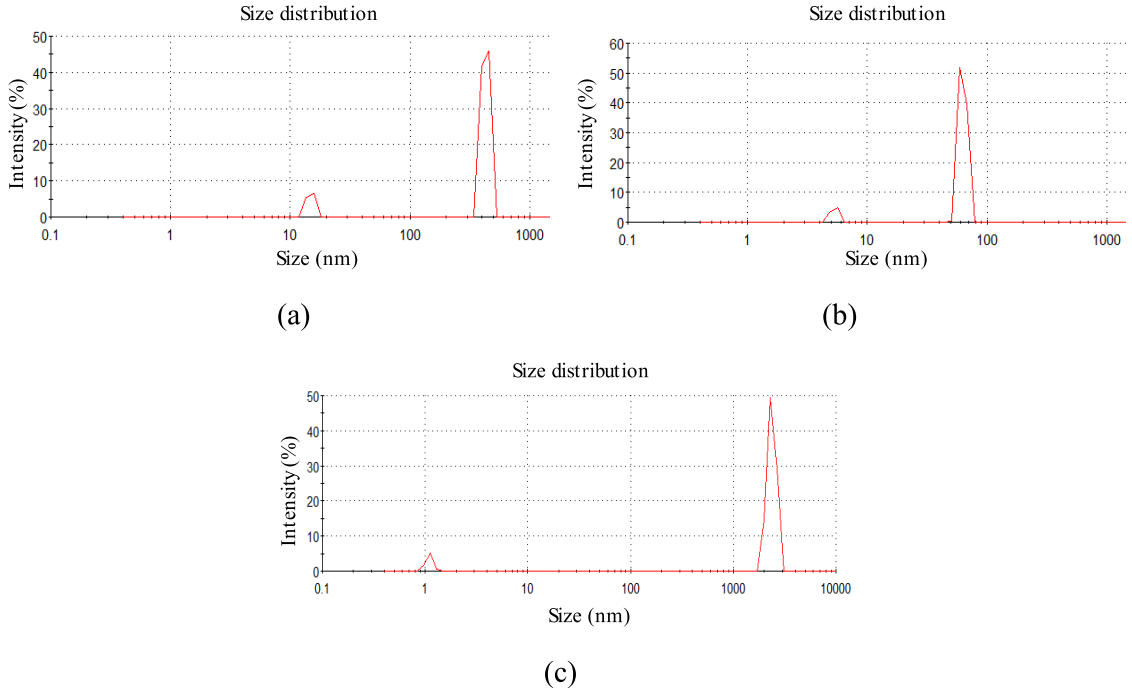

Figure 3. Size distribution of PDVB-NPs: (a) PDVB-0.045, (b) PDVB-0.45, and (c) PDVB-4.5.

https://dx.doi.org/10.1021/acs.langmuir.0c02991
Langmuir 2021, 37, 376−384

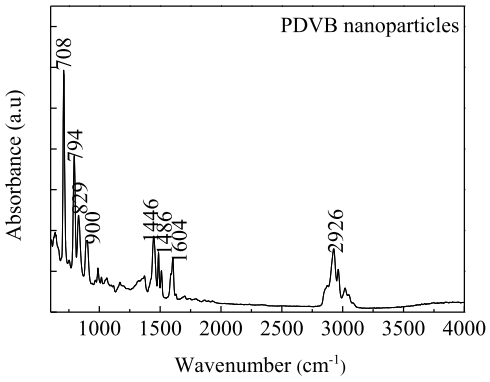

Figure 4. FT-IR spectrum of PDVB-NPs under the attenuated-total reflection (ATR) mode.

Figure 5 shows the variation of the dynamic viscosities of the PDVB-NP solutions with the PDVB-NP concentration for three different sizes of PDVB-NPs. The dynamic viscosity is a linearly increasing function of the PDVB-NP concentration, as expected, for dilute solutions. For the same PDVB-NP concentration, the solution with PDVB-4.5 has the smallest viscosity, and the solution with PDVB-0.045 has the largest viscosity. Such a trend suggests that the average particle size of PDVB-4.5 is the smallest, and the average particle size of PDVB-0.045 is the largest. This result is consistent with the result obtained from the particle-size analysis.

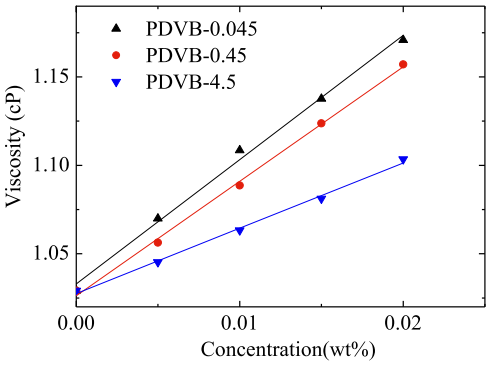

Figure 5. Concentration dependence of the dynamic viscosities of the PDVB-NP solutions with different PDVB-NPs.

Figure 6 depicts the energy-dispersive X-ray (EDX) spectra of the coated papers, from which the atomic fractions of the elements were determined and listed in corresponding figures. All coated papers contain oxygen, calcium, aluminum, silicon, magnesium, and sodium, suggesting that starch fluid (C), calcium carbonate, sodium corboxymethyl cellulose, kaolinite (Al, Si), and talcum (Si, Mg) are there in the coating layer. The Au peak was attributed to the gold coating, and the Cu peak was ascribed to the Cu tape used to fix the specimens for the SEM imaging and EDX analysis.

Three different liquids of DI water, glycerol, and mercury were used in the measurement of the contact angle on the coating layers. Table 1 lists the measured contact angles over the coating layers made from three different PDVB-NPs. In general, all of the contact angles were larger than 148°,

Table 1. Contact Angles of Three Different Liquids on the Coating Layers

PDVB-NPs in coating layer	contact angle (deg)		
	DI water	glycerol	mercury
PDVB-0.045	152.90 ± 1.20	149.50 ± 0.64	163.54 ± 0.47
PDVB-0.45	152.08 ± 1.01	149.12 ± 0.78	163.06 ± 0.57
PDVB-4.5	151.57 ± 0.67	148.66 ± 0.84	162.52 ± 0.39

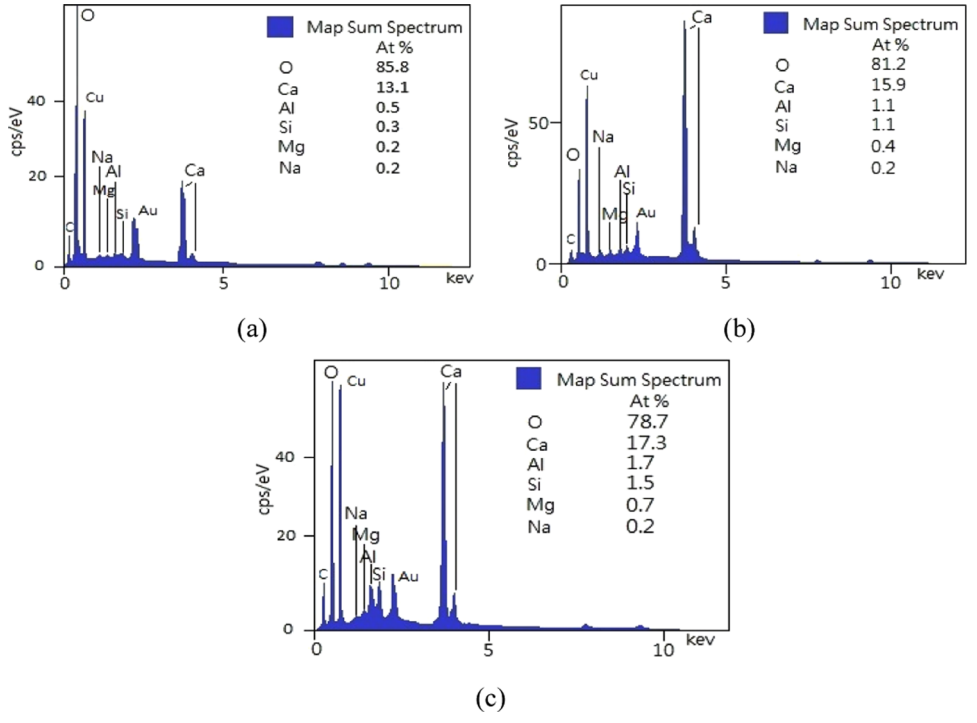

Figure 6. EDX spectra of the coated papers: (a) HW paper, (b) LW paper, and (c) SW paper.

https://dx.doi.org/10.1021/acs.langmuir.0c02991
Langmuir 2021, 37, 376−384

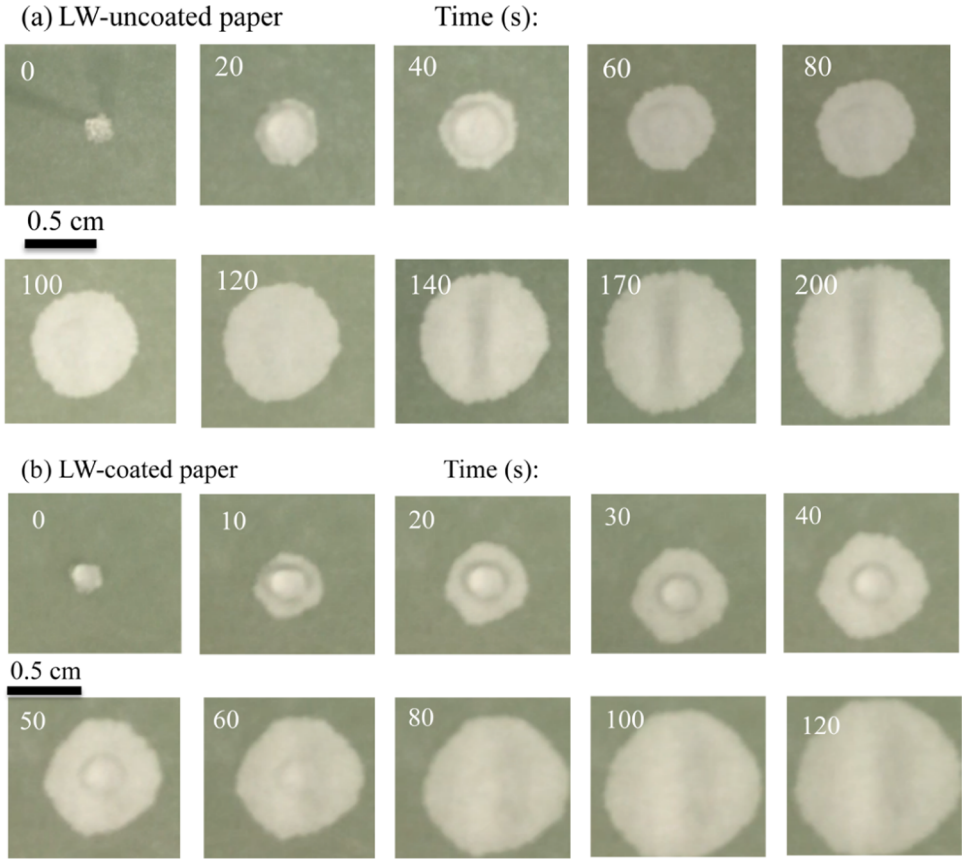

Figure 7. Optical images of the spreading of a water droplet on the uncoated surface of LW papers at different instants: (a) with an uncoated backside and (b) with a coated backside.

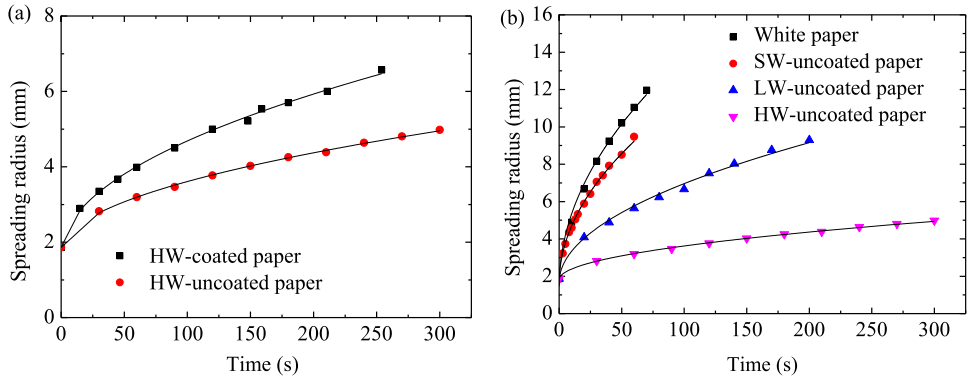

Figure 8. Temporal variation of the spreading size for the spreading of a DI water droplet on the uncoated surface of different papers at 25 °C: (a) HW papers with and without back-surface coating and (b) papers without back-surface coating.

suggesting that the coating layers exhibited superhydrophobic characteristics. Note that there is no statistical difference among the contact angles for the same liquid on the three different coating layers, even though the contact angle decreases slightly with the decrease of the average size of PDVB-NPs (the increase of the amount of AIBN).

Figure 7 shows optical images of the spreading of a water droplet on the uncoated surface of an LW paper with and without back-surface coating at different instants, respectively. It is evident that the spreading size increases with the increase of time for both papers in accord with the wetting behavior of water on a cellulose-based paper. However, the water droplet on the surface of the LW-coated paper spread much faster than that on the surface of the LW-uncoated paper. Such behavior reveals the effect of the back-surface coating on the spreading behavior of water droplets on the uncoated surface.

Using ImageJ, we analyzed the optical images and calculated the spreading size at different instants. Figure 8a shows the temporal variation of the spreading size for the spreading of water droplets on the uncoated surfaces of HW-coated and uncoated papers. More results are given in the Supporting Information (Figure S1). It is evident that the spreading size is a nonlinearly increasing function of the spreading time. The spreading front for the spreading on the papers without back-surface coating moved at a speed less than that with back-surface coating at the same spreading time for both types of papers. Such results support the fact that the back-surface

https://dx.doi.org/10.1021/acs.langmuir.0c02991
Langmuir 2021, 37, 376−384

coating plays an important role in the spreading behavior of water droplets on the uncoated surface of the papers.

For the uncoated papers, the spreading on the white newspaper is the fastest, and the spreading on the HW-uncoated paper is the slowest (Figure 8b). Such results demonstrate the structural effect on the spreading of water droplets.

It is known that the coating thickness is dependent on the spin speed. Figure S2 presents the temporal evolution of the spreading size of a water droplet on LW papers with the coating layers made at different spin speeds. It is evident that there is no significant difference in the spreading kinetics of the water droplets on the papers with the back-surface coating made with the spin speed in a range of 400−800 rpm.

Krämer[24] introduced intrinsic viscosity of a cellulosic solution, $[\eta]$, as

$$[\eta] = \lim_{c\to 0}\left[\frac{1}{c}\ln\left(\frac{\eta}{\eta_0}\right)\right] \tag{1}$$

where η and η_0 are the viscosities of the solution and pure solvent, respectively, and c is the concentration. The correlation between the intrinsic viscosity of the solution of long-chain molecules and the molecular weight of the long-chain molecules can be expressed as[25]

$$[\eta] = KM^a \tag{2}$$

with K being a constant and a being a power index. Both k and a are dependent on the particular polymer-solvent system.

For a dilute solution, eqs 1 and 2 yield

$$[\eta] = \lim_{c\to 0}\frac{1}{c}\left(\frac{\eta}{\eta_0} - 1\right) = KM^a \tag{3}$$

The dynamic viscosity of the solvent as measured by the Cannon-Ubbelohde 6963S glass viscometer is 1.029 cP. Using the results in Figure 5 and η_0 = 1.029 cP, we obtain the intrinsic viscosities of 8.80 ± 0.06, 5.18 ± 0.05, and 3.21 ± 0.03 dL/g for the solutions made from PDVB-0.045, PDVB-0.45, and PDVB-4.5, respectively. According to eq 3, the molecular weight of PDVB-4.5 is the smallest, and the molecular weight of PDVB-0.045 is the largest. Increasing the fraction of AIBN decreases the molecular weight of PDVB-NPs. From Figure 3, we note that the average particle size of the PDVB-NPs decreases with the increase of the fraction of AIBN. Thus, the smaller the molecular weight of PDVB-NPs, the smaller is the average particle size of the PDVB-NPs.

The results in Figure 8 suggest that the microstructures (porous structures) of the PDVB-NP-coated and uncoated papers are likely different. Figures S3−S11 present SEM images of all papers with and without back-surface coating. It is evident that there is no significant difference in local microstructures between the uncoated papers and the uncoated surface of the corresponding papers with the back-surface coating. However, there are PDVB-NPs presented in the coated papers, suggesting the penetration of PDVB-NPs into the papers during the spin-coating. The presence of PDVB-NPs in the coated papers allows for the trapping of local air bubbles, which reduce the resistance to the water flow in the papers. Note that there are significant differences in local microstructures between different types of papers. It is the difference in local microstructures, which contributes to the difference in the temporal evolution of the spreading of water droplets.

Various models[19,26−28] have been developed to analyze the spreading of liquid droplets on rough and porous surfaces. Realizing the penetration of liquid into a porous substrate, Gillespie[19] and Clarke et al.[28] pointed out the need to consider the flow in the porous substrate. Gillespie[19] correlated Darcy's law with the liquid concentration for the flow of a gas−liquid mixture in a paper for the liquid spreading in the paper, and Clarke et al.[28] correlated surface tension with the pressure gradient in Darcy's law for the analysis of the liquid penetration into a porous substrate. None of the studies has analyzed the liquid flow, contributing to the spreading of liquid in a porous substrate.

For the liquid flow in a porous material, the equilibrium equation is[29]

$$\nabla^2 p = \frac{\mu\phi(c_f + c_\phi)}{k}\frac{\partial p}{\partial t} \tag{4}$$

and the relation between the pressure gradient and the flow velocity is

$$\mathbf{u} = -\frac{k}{\mu}\nabla p \tag{5}$$

where p is the pressure, $\mathbf{u}$ is the flow velocity, μ is the apparent viscosity of the liquid in the porous material, k is the permeability of the porous material, ϕ is the porosity of the porous material, and c_f and c_g are the compressibility of the liquid and the "pore compressibility" of the porous material, respectively.

The flow flux, which is proportional to the flow velocity, can be expressed as

$$\mathbf{J} = \mathbf{nu} \tag{6}$$

where n is the number of water molecules per unit volume. In this experiment, the total number of water molecules per unit thickness remains constant as $n_0\pi r_0^2$, where n_0 and r_0 are the initial number of water molecules per unit volume and the initial spreading radius, respectively. According to Figure 7, the spreading radius increases with the spreading time, suggesting that the average number of water molecules per unit volume decreases with increasing spreading time. Therefore, it is reasonable to assume the presence of the gradient of water molecules, which correlates with the flow flux as

$$\mathbf{J} = -\alpha\nabla n \tag{7}$$

where α is the diffusion coefficient.

Using eqs 4−7 and assuming that n approaches the reference number of water molecules per unit volume, n_R, one obtains

$$n = n_R\phi(c_f + c_\phi)p \tag{8}$$

$$\alpha = \frac{k}{\mu\phi(c_f + c_\phi)} \tag{9}$$

and eq 4 is rearranged as

$$\frac{\partial n}{\partial t} = \alpha\nabla^2 n \tag{10}$$

Consider a water droplet of radius r_0 spreading on an infinite large paper. Note that r_0 is approximately equal to the radius of the contact zone at t = 0, as shown in Figure 7. At the initial

https://dx.doi.org/10.1021/acs.langmuir.0c02991
Langmuir 2021, 37, 376−384

time, the water drop is distributed homogeneously on the paper within radius r_0. That is

$$n(r \leq r_0,\ t = 0) = n_0 \tag{11}$$

$$n(r > r_0,\ t = 0) = 0 \tag{12}$$

The solution of n is[30]

$$n(r,\ t) = \frac{n_0}{2\alpha t} e^{-r^2/4\alpha t} \int_0^{r_0} e^{-x^2/4\alpha t} I_0\left(\frac{xr}{2\alpha t}\right) x\mathrm{d}x \tag{13}$$

where $I_0(\bullet)$ is the first kind of the modified Bessel function of the zeroth order. Note that the ratio of $k/\mu\phi(c_f + c_\phi)$ or α is a constant for a given system of porous structure and liquid at a given temperature. The shape of the water drop is determined by eq 13 when n is equal to 0.001 n_0 for $t > 0$.

Using eq 13 to curve fit the curves in Figures 7, S1, and S12−S15, we can obtain the values of α for the spreading of water droplets on the coated and uncoated papers used in this work in the temperature range of 25−55 °C. For comparison, the fitting curves are also included in the corresponding figures. It is evident that eq 13 can well describe the spreading behavior of water droplets on the coated and uncoated papers. The fitting results reveal that the temperature dependence of the spreading size of the water droplets can be expressed as

$$r - r_0 = (\chi\alpha t)^{1/2} \tag{14}$$

with χ as a proportional constant.

According to eq 9, the parameter, α, is inversely proportional to the apparent viscosity of the liquid spreading on the papers, μ, the porosity of the papers, ϕ, and the summation of the compressibility of the liquid and the pore compressibility of the papers, $c_f + c_\phi$, and proportional to the permeability of the papers, k. The parameters of ϕ, $(c_f + c_\phi)$, and k are related to the porous structures of the papers and the mechanical properties of water and the papers, which are independent of temperature. The apparent viscosity, μ, exhibits the temperature dependence as

$$\mu = \mu_0 e^{Q/RT} \tag{15}$$

with Q being the energy barrier (nominal activation energy) for the flow of water in the papers, R is the gas constant, and T is the absolute temperature. Thus, we have

$$\alpha = \alpha_0 e^{-Q/RT} \tag{16}$$

where α_0 is a pre-exponential factor and proportional to $k/\phi(c_f + c_g)$, i.e., it depends on the structures of the papers. The temperature dependence of $(\chi\alpha)^{-1}$ for the coated and uncoated papers used in this work, in which the PVDB coatings with different particle sizes were used, is presented in Figure S16. Using eq 16 to fit the curves in Figure S1, we obtain the energy barrier and the pre-exponential factor. Figure S17 shows the variation of the energy barrier and pre-exponential factor, $\chi\alpha_0$, with the amount of AIBN used in the preparation of the PVDB nanoparticles for the spreading of water droplets on HW, LW, and SW papers.

According to Figure S17, increasing the amount of AIBN (decreasing the size of the PVDB nanoparticles) leads to the decrease of the energy barrier for the spreading/flow of water, which reveals that the smaller the size of the PVDB nanoparticles used in the back-surface coating, the smaller is the energy barrier for water to flow in the porous papers. This behavior can be likely attributed to the deep penetration of small PVDB nanoparticles into the porous papers during the spin-coating, which produces a large amount of "tiny" air bubbles and a large fraction of a hydrophobic surface due to the large ratio of the surface area to volume.

The increase in the amount of small PVDB nanoparticles in the porous papers can also cause decrease in the permeability of the porous papers and the pre-exponential factor accordingly. According to Figure S16, we note that there are differences in the pre-exponential factors among the HW, LW, and SW papers. Such differences are associated with the differences in the porous structures, permeabilities, and compressibilities of the porous papers. The spreading of liquid in a porous material is much more complicated than the spreading on a rough, solid surface.

Figure 9 presents the comparison of the energy barrier and the pre-exponential factors for the spreading of water droplets

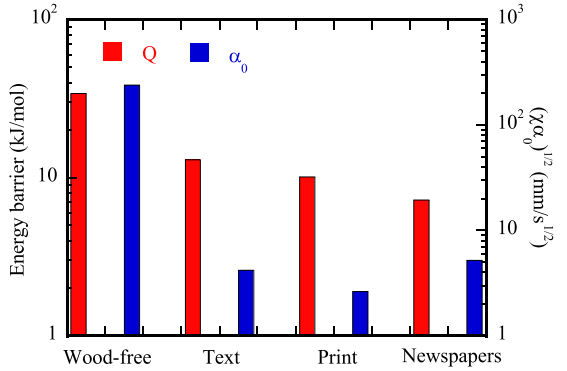

Figure 9. Spreading characteristics of water droplets on four different papers.

on four different types of papers without back-surface coating. Again, we observe the dependence of the energy barrier and the pre-exponential factor on the papers used in the tests. There exists fluid−structure interaction for the spreading of liquid in a porous material.

4. SUMMARY

In summary, we have demonstrated the effects of back-surface coating and the size of PVDB nanoparticles on the spreading of water droplets in different types of papers. Using Darcy's law, we have developed a relationship for the temporal evolution of the spreading size of a liquid droplet on a porous material. Such a relationship is supported by the experimental results of the spreading of water droplets, which were dripped on the uncoated surface of the different types of papers with and without back-surface coating. The porous structure, permeability, and compressibility of the porous papers as well as the back-surface coating play important roles in the spreading of water droplets.

Using the relationship and the experimental data, we have calculated the energy barrier and the pre-exponential factor for the spreading of water droplets on heavy-weight, light-weight, and slight-weight papers. The energy barrier for all of the three types of papers exhibits similar trend to the pre-exponential factor. Decreasing the size of the PVDB nanoparticles for the back-surface coating leads to the decrease of the energy barrier and the pre-exponential factor. Such a trend suggests that the smaller the size of the PVDB nanoparticles used in the surface coating, the smaller is the energy barrier for water to flow in the porous papers.

https://dx.doi.org/10.1021/acs.langmuir.0c02991
Langmuir 2021, 37, 376−384

The results presented in this work demonstrate a feasible method to use the back-surface coating instead of top-surface coating to control the wettability of papers. It allows for multilayer back-surface coating with the first layer consisting a mixture of quantum dots and superhydrophobic PDVB nanoparticles for fluorescent anticounterfeiting labels. Also, one can use nanoparticles of different sizes to confine/regulate the spreading/flow of liquids on/in porous materials.

■ ASSOCIATED CONTENT

Supporting Information

The Supporting Information is available free of charge at https://pubs.acs.org/doi/10.1021/acs.langmuir.0c02991.

Detailed information of the papers and the abbreviations used in this work (Tables S1 and S2), the temporal evolution of the spreading size of a water droplet on different papers at 25 °C (Figure S1), the temporal evolution of the spreading size of a water droplet on LW papers with a coating layer made at different spin speeds (Figure S2), SEM images of coated and uncoated papers (Figures S3−S11), the temporal evolution of the spreading size of a water droplet on HW papers at different temperatures (Figures S12−S15), the temperature dependence of $(\chi\alpha)^{-1}$ with and without back-surface coating (Figure S16), and the effect of the amount of AIBN (size of PVDB nanoparticles) on the spreading characteristics of water droplets on heavy-weight, light-weight, and slight-weight papers (Figure S17) (PDF)

■ AUTHOR INFORMATION

Corresponding Author

Sanboh Lee − *Department of Materials Science and Engineering, National Tsing Hua University, Hsinchu 30013, Taiwan;* orcid.org/0000-0001-5947-8189; Phone: +88635719677; Email: sblee@mx.nthu.edu.tw

Authors

Ching-Bin Lin − *Mechanical and Electro-Mechanical Engineering, Tamkang University, New Taipei City 251301, Taiwan*

Han-Sen Chang − *Department of Materials Science and Engineering, National Tsing Hua University, Hsinchu 30013, Taiwan*

Yulin Zhang − *Materials Program, Department of Chemical and Materials Program, University of Kentucky, Lexington, Kentucky 40506, United States*

Fuqian Yang − *Materials Program, Department of Chemical and Materials Program, University of Kentucky, Lexington, Kentucky 40506, United States;* orcid.org/0000-0001-6277-3082

Complete contact information is available at: https://pubs.acs.org/10.1021/acs.langmuir.0c02991

Notes

The authors declare no competing financial interest.

■ ACKNOWLEDGMENTS

S.L. would like to thank the Ministry of Science and Technology, Taiwan, for the financial support. The authors are also indebted to the Taiwan Instrument Research Institute for providing instruments.

■ REFERENCES

(1) Gu, C. D.; Wang, X. Q.; Zhang, J. L.; Tu, J. P. Super antiwetting surfaces for mitigating drag-out of deep eutectic solvents. *ACS Appl. Mater. Interfaces* **2018**, *10*, 24209−24216.

(2) Tsuruki, Y.; Sakai, M.; Isobe, T.; Matsushita, S.; Nakajima, A. Static and dynamic hydrophobicity of alumina-based porous ceramics impregnated with fluorinated oil. *J. Mater. Res.* **2014**, *29*, 1546−1555.

(3) Feng, X. J.; Jiang, L. Design and creation of superwetting/antiwetting surfaces. *Adv. Mater.* **2006**, *18*, 3063−3078.

(4) Zhang, J.; Gu, C.; Tu, J. Robust slippery coating with superior corrosion resistance and anti-icing performance for AZ31B Mg alloy protection. *ACS Appl. Mater. Interfaces* **2017**, *9*, 11247−11257.

(5) Bahadur, V.; Mishchenko, L.; Hatton, B.; Taylor, J. A.; Aizenberg, J.; Krupenkin, T. Predictive model for ice formation on superhydrophobic surfaces. *Langmuir* **2011**, *27*, 14143−14150.

(6) Liu, C.; Wang, N.; Long, Y. Multifunctional overcoats on vanadium dioxide thermochromic thin films with enhanced luminous transmission and solar modulation, hydrophobicity and anti-oxidation. *Appl. Surf. Sci.* **2013**, *283*, 222−226.

(7) Yang, W.; Li, J.; Zhou, P.; Zhu, L.; Tang, H. Superhydrophobic copper coating: Switchable wettability, on-demand oil-water separation, and antifouling. *Chem. Eng. J.* **2017**, *327*, 849−854.

(8) Luo, H.; Yin, S.; Zhang, G.; Tang, Q.; Gen, J.; Huang, S. Study of superhydrophobic surface in self-cleaning of magnetorheological fluid. *J. Mater. Sci.* **2018**, *53*, 1769−1780.

(9) Kim, M.-K.; Cha, H.; Birbarah, P.; Chavan, S.; Zhong, C.; Xu, Y.; Miljkovic, N. Enhanced jumping-droplet departure. *Langmuir* **2015**, *31*, 13452−13466.

(10) Roach, P.; Shirtcliffe, N. J.; Newton, M. I. Progess in superhydrophobic surface development. *Soft Matter* **2008**, *4*, 224−240.

(11) Samyn, P. Wetting and hydrophobic modification of cellulose surfaces for paper applications. *J. Mater. Sci.* **2013**, *48*, 6455−6498.

(12) Balu, B.; Kim, J. S.; Breedveld, V.; Hess, D. W. Design of Superhydrophobic Paper/cellulose Surfaces via Plasma Enhanced Etching and Deposition. In *Contact Angle, Wettability and Adhesion*; Mittal, K. ed., Koninklijke Brill NV: Leiden, Neitherlands, 2009; *6* pp 235−250.

(13) Li, L.; Breedveld, V.; Hess, D. W. Design and fabrication of superamphiphobic paper surfaces. *ACS Appl. Mater. Interfaces* **2013**, *5*, 5381−5386.

(14) Zhang, S.; Li, W.; Wang, W.; Wang, S.; Qin, C. Reactive superhydrophobic paper from one-step spray-coating of cellulose-based derivative. *Appl. Surf. Sci.* **2019**, *497*, No. 143816.

(15) Jiang, L.; Tang, Z.; Clinton, R. M.; Hess, D. W.; Breedveld, V. Fabrication of highly amphiphobic paper using pulp debonder. *Cellulose* **2016**, *23*, 3885−3899.

(16) Han, J.; Krochta, J. Wetting properties and water vapor permeability of whey-protein-coated paper. *Trans. ASAE* **1999**, *42*, 1375−1382.

(17) Modaressi, H.; Garnier, G. Mechanism of wetting and absorption of water droplets on sized paper: Effects of chemical and physical heterogeneity. *Langmuir* **2002**, *18*, 642−649.

(18) Kwon, T.; Hopkins, A.; O'Donnell, S. Dynamic scaling behavior of a growing self-affine fractal interface in a paper-towel-wetting experiment. *Phys. Rev. E* **1996**, *54*, No. 685.

(19) Gillespie, T. The spreading of low vapor pressure liquids in paper. *J. Colloid Sci.* **1958**, *13*, 32−50.

(20) Rosenholm, J. B. Liquid spreading on solid surfaces and penetration into porous matrices: Coated and uncoated papers. *Adv. Colloid Interface Sci.* **2015**, *220*, 8−53.

(21) Chang, C. Manufacturing and Application of Nano-Superhydrophobic Polydivinylbenzene Particulates. Master Thesis; Department of Mechanical and Electo-Mechanical Engineering,Tamkang University: New Taipei City, Taiwan, 2016.

(22) Jafari, T.; Moharreri, E.; Toloueinia, P.; Amin, A. S.; Sahoo, S.; Khakpash, N.; Noshadi, I.; Alpay, S. P.; Suib, S. L. Microwave-assisted synthesis of amine functionalized mesoporous polydivinylbenzene for CO_2 adsorption. *J. CO_2 Util.* **2017**, *19*, 79−90.

(23) Nuasaen, S.; Tangboriboonrat, P. Highly charged hollow latex particles prepared via seeded emulsion polymerization. *J. Colloid Interface Sci.* **2013**, *396*, 75−82.
(24) Krämer, E. O. Molecular Weights of celluloses and cellulose derivates. *Ind. Eng. Chem.* **1938**, *30*, 1200−1203.
(25) Hiemenz, P. C.; Lodge, T. P. *Polymer Chemistry*, 2nd ed.; CRC Press: Boca Raton, FL, 2007; pp 336−339.
(26) Davis, S. H.; Hocking, L. Spreading and imbibition of viscous liquid on a porous base. *Phys. Fluids* **1999**, *11*, 48−57.
(27) Shuttleworth, R.; Bailey, G. The spreading of a liquid over a rough solid. *Discuss. Faraday Soc.* **1948**, *3*, 16−22.
(28) Clarke, A.; Blake, T.; Carruthers, K.; Woodward, A. Spreading and imbibition of liquid droplets on porous surfaces. *Langmuir* **2002**, *18*, 2980−2984.
(29) Zimmerman, R. W. *Fluid Flow in Porous Media*; World Scientific Publishing Europe Limited, 2018.
(30) Lee, S.; Lee, H.; Lee, I.; Tseng, C. Ink diffusion in water. *Eur. J. Phys.* **2004**, *25*, 331−336.

https://dx.doi.org/10.1021/acs.langmuir.0c02991
Langmuir 2021, 37, 376−384